

# Cramer-Rao Lower Bounds for Visible Light Communication based Vehicle Localization Methods

Burak Soner, *Student Member, IEEE*, and Sinem Coleri, *Senior Member, IEEE*,

**Abstract**—Recent works on visible light communication (VLC) based vehicle localization methods using VLC signals from head/tail LED lights for positioning report cm-level accuracy and near-kHz rates, which can enable collision avoidance and platooning for safer autonomous driving. However, existing analyses of these methods are not comparable and are inconclusive since they assume different system models and consider limited simulations. In this paper, we analyze the theoretical performances of four state-of-the-art (SoA) methods which measure physical VLC system parameters (e.g., propagation distance) using phase-difference-of-arrival (PDoA), roundtrip-time-of-flight (RToF), and single/dual receiver angle-of-arrival (AoA1/AoA2) characteristics of received signals respectively, and estimate position based on these parameters and geometric relations (e.g., triangulation). Specifically, we derive the Cramer-Rao lower bound (CRLB) on positioning accuracy for each method with respect to measured parameters, simulate their parameter measurement procedures under realistic driving scenarios, and evaluate their CRLBs using these simulated measurements. Results show that the current SoA PDoA based method fails to provide cm-level accuracy under any realistic scenario considering the  $\leq 1$  MHz bandwidth of current head/tail LED lights. The AoA1 method provides cm-level accuracy for close range platooning, but its high-sensitivity geometry causes accuracy degradation at high distances. RToF and AoA2 methods provide cm-level accuracy under low to moderate VLC channel noise for all scenarios within 10 m distance, theoretically proving the feasibility of VLC based vehicle localization for collision avoidance and platooning.

**Index Terms**—autonomous vehicles, collision avoidance, platooning, visible light positioning, cramer-rao bounds

## I. INTRODUCTION

Collision avoidance and platooning are essential applications for safe and efficient autonomous driving [1]. For full autonomy, these applications require vehicle-to-vehicle localization with cm-level accuracy and  $>50$  Hz rate [2, 3]. Conventional vehicle localization methods using repurposed sensor-based object detector/trackers (e.g., LIDARs, cameras) fail to meet these stringent requirements due to sensor rate limitations and high computational complexity, necessitating complementary solutions [4]. Vehicle localization based on visible light positioning (VLP), which uses received visible light communication (VLC) signals from modulated vehicle head/tail LED lights for positioning, fundamentally promises the required accuracy and rate for these applications, thus, is a suitable complementary addition to the sensor-based autonomous driving system of the future [5].

Burak Soner and Sinem Coleri are with the Department of Electrical and Electronics Engineering, Koc University, 34450 Istanbul, Turkey (e-mail: bsoner16@ku.edu.tr, scoleri@ku.edu.tr). Burak Soner is also with Koc University Ford Otosan Automotive Technologies Laboratory (KUFOTAL), Istanbul, Turkey. The authors acknowledge the support of Ford Otosan and the Scientific and Technological Research Council of Turkey EU CHIST-ERA grant # 119E350.

VLP methods use VLC signals for position estimation typically via two-step algorithms: First, received noisy VLC signals are used for measuring physical system parameters (e.g., angle of direction line or propagation distance from a transmitter) with a certain level of accuracy. Then, these measured physical parameters are used for estimating the position of the VLC transmitter (TX) relative to the VLC receiver (RX) via geometric relations (e.g., multi-lateration, triangulation). Positioning accuracy in these two-step algorithms is therefore jointly determined by the accuracy in parameter measurement and the sensitivity of the underlying geometric relations to errors in those measurements. While single-step estimators (i.e., no parameter measurement, direct localization based on RX signals) also exist [6], they are only useful when the relations between the received signals and the measured physical parameters get distorted due to inter-symbol interference by significant non-line-of-sight (LoS) components from specular and reflective surfaces, e.g., in indoor environments. Since the vehicular VLC channel is LoS-dominant for TX-RX distances that are relevant in collision avoidance and platooning [7, 8], vehicular VLP methods use two-step algorithms for estimating the relative positions of VLC TXs. Estimating the positions of two vehicular VLC TXs, i.e., two head or two tail lights, suffices for 2D localization of road vehicles [9].

Existing VLC based vehicle localization methods that promise the required accuracy and rate utilize the following physical parameters: differences in propagation distances [10], absolute propagation distances [11, 12], and angles of direction lines [9, 13] from TXs to RXs. Each method proposes a different procedure for measuring one of these parameters, which are then used for position estimation through geometric relations. In [10], phase-difference-of-arrival (PDoA) of two RX VLC signals are used for measuring the differences in propagation distances ( $\Delta d_p$ ) from two TXs, which are then used for estimating the relative TX positions with cm-level accuracy for longitudinally parallel vehicles. In [11], roundtrip-time-of-flight (RToF) of a VLC message between two VLC units on two vehicles is used for measuring the absolute propagation distance ( $d_p$ ), which is extended to position estimation at cm-level accuracy in [12] when the adjacent VLC units on both vehicles are also used. In [13], two time-consecutive angle-of-arrival (AoA) measurements from a single quadrant-photodiode based VLC receiver and heading and speed information from vehicle sensors are used for cm-level position estimation via triangulation with angles of direction lines. This method is improved in [9] by removing the heading and speed sensors and using two such AoA-sensing VLC receivers, i.e. one on each head/tail light, for regular triangulation. While these existing works claim cm-level accuracy and

>50 Hz rate, they do so based on limited simulation scenarios: Their results are not comparable since each one assumes a different system model and VLC channel condition, and they are inconclusive due to the lack of theoretical analyses, casting doubt on the efficacy of vehicular VLP under general realistic road and VLC channel conditions.

In this paper, we analyze and compare the theoretical performances of these four state-of-the-art VLC based vehicle localization methods [9, 10, 12, 13] under a common system model for realistic driving scenarios. First, we present the geometric relations between the TX position and the measured physical parameters used by each method, and derive the Cramer-Rao lower bounds (CRLB) on position accuracy for each relation. We derive the CRLB specifically with respect to the measured parameters rather than to the received signals to obtain expressions that apply to all possible parameter measurement procedures. Then, we simulate the physical parameter measurement procedure proposed by each state-of-the-art method under a common finite-propagation-delay, LoS, additive white Gaussian noise (AWGN) VLC channel model for realistic road and VLC channel conditions in collision avoidance and platooning scenarios, and evaluate the respective CRLB on positioning accuracy for each method based on these simulated parameter measurements. Our main contributions are summarized as follows:

- We derive the CRLBs on positioning accuracy for the four state-of-the-art VLC based vehicle localization methods [9, 10, 12, 13] based on their physical parameter observations. Since these bounds specifically express the sensitivity of the geometric relations between the physical parameters and the TX position, they apply to all methods that use one of the subject geometries, regardless of the parameter measurement procedure (e.g., a new PDoA measurement procedure can be evaluated for positioning accuracy using the CRLB we derive based on [10]). While similar theoretical analyses exist for localization methods that consider indoor luminaries [6, 14], this paper provides the theoretical analysis of vehicle localization methods for the first time in the literature.
- We represent the parameter measurement procedures proposed by the considered methods (i.e.,  $\Delta d_p$  measurement using PDoA [11],  $d_p$  measurement using RTToF [10], and angle of direction line [9, 13] and relative heading and speed measurement [13] using AoA and sensor data) under a common system model and simulate their performances (i.e., we sample their variance for use in evaluating the CRLB) under the same road and VLC channel conditions for realistic collision avoidance and platooning scenarios, for the first time in the literature.
- We use the simulated parameter measurements to evaluate and compare the CRLBs on positioning accuracy for the four methods and theoretically prove that the RTToF [11] and AoA [9] based methods can reliably attain cm-level accuracy and 200 Hz rate vehicle localization under realistic general driving scenarios, thus, can satisfy the requirements for collision avoidance and platooning, for the first time in the literature.

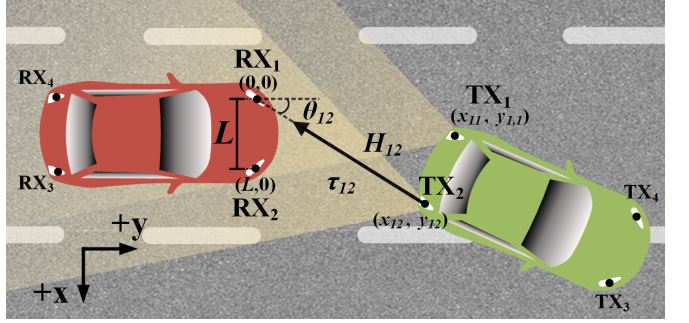


Fig. 1. System model: The ego vehicle (red) estimates the positions of two TX units on the target vehicle (green), i.e.,  $(x_{11}, y_{11})$  and  $(x_{12}, y_{12})$ , for vehicle localization.  $H_{12}$  is the channel gain,  $\tau_{12}$  is the propagation time and  $\theta_{12}$  is the AoA between TX 2 and RX 1.  $L$  is the RX separation.

The rest of the paper is organized as follows. System model assumptions, the common mathematical model of the received VLC signals, and the problem definition for VLC/VLP based vehicle localization using these received signals are presented in Section II. The details of the four state-of-the-art VLC based vehicle localization methods are summarized, and the respective CRLBs are derived in Section III. The parameter measurement procedures of each method are simulated and their respective CRLBs are evaluated using those simulated measurements for collision avoidance and platooning scenarios in Section IV. Our conclusions are presented in Section V.

## II. SYSTEM DESCRIPTION

### A. System Model Assumptions

The model is based on the following assumptions (A#):

- A1: Vehicles are equipped with VLC units containing LED TXs and photodiode-based RXs on their head and tail lights (i.e., 4 VLC units in total), sustaining reliable LoS communication with each other. Received VLC signals are used for positioning VLC TXs.
- A2: The content of the VLC messages are arbitrary and can be used for the positioning algorithm.
- A3: Transmissions by the VLC units do not interfere. This can be achieved via special medium access control mechanisms, e.g., by assigning each unit to a separate frequency band [15].
- A4: Vehicles cruise on piecewise-flat roads, i.e., their pitch angle with respect to the horizon is the same. This assumption, which reduces the 3D positioning problem to 2D (i.e., road plane), is reasonable for collision avoidance and platooning scenarios where vehicles are within 1-20 m of each other driving at  $\geq 30$  km/h [16, 17].

We call the vehicle that is being positioned the “target” vehicle, and the vehicle that is estimating the position the “ego vehicle”. Fig. 1 depicts this system model for the case of a target vehicle (green) being followed by an ego vehicle (red). However, both vehicles can take either role at a given time, in any orientation, since they have the same configuration.

### B. Mathematical Model of Received VLC Signals

We consider the following received VLC signal model:

$$r_i(t) = \sum_j [H_{ij} s_j(t - \tau_{ij})] + \mu_i(t) \quad (1)$$

where  $t$  is time,  $i, j \in \{1, 2, 3, 4\}$  are indices for RXs and TXs on vehicle lights respectively,  $r_i$  is the received photocurrent signal,  $s_j$  is the transmitted photocurrent signal,  $\mu_i$  is the photocurrent AWGN, and  $H_{ij}$  and  $\tau_{ij}$  are respectively the geometric channel gain and the finite propagation time from TX  $j$  to RX  $i$ . Since TX signals are directional, only two TXs on a given face of the target vehicle contribute to Eqn. (1) for a given RX on the ego vehicle, i.e.,  $j$  is either  $\in \{1, 2\}$  or  $\in \{3, 4\}$  for a given  $i \in \{1, 2, 3, 4\}$  depending on vehicle orientation, and these two TX components, e.g.,  $s_1$  from  $s_2$ , can be separated in  $r_i$  as per assumption A3.

Expressions for  $H_{ij}$ ,  $\tau_{ij}$  and  $\mu_i$  rely on the point-source approximation of TXs from the perspective of RXs: The minimum RX-TX distance at which the inverse square law for received optical power for point-sources starts to hold (i.e., photometric / far-field / cross-over distance) is  $\approx 50$  cm for automotive LED lights [18–20]. Since this is smaller than the 1 m minimum distance assumed in A4, TXs are safely assumed as point sources in this paper, which simplifies expressions for  $H_{ij}$ ,  $\tau_{ij}$  and  $\mu_i$ . The channel gain  $H_{ij}$  can be expressed as:

$$H_{ij} = \gamma_i \rho_i(\theta_{ij}) \iint_{S_{ij}} \gamma_j \rho_j(S) dS, \quad S_{ij} \propto \frac{A_i \cos(\theta_{ij})}{\sqrt{x_{ij}^2 + y_{ij}^2}} \quad (2)$$

where  $\rho_j$  and  $\rho_i$  are the normalized positive-definite TX beam pattern and RX “reception” pattern respectively,  $\gamma_j$  and  $\gamma_i$  are the TX electrical-to-optical gain and RX optical-to-electrical (i.e., photodiode) sensitivity respectively,  $S_{ij}$  is the solid angle subtended by the active area of the RX  $i$  with respect to TX  $j$  [21], and  $\theta_{ij}$  and  $(x_{ij}, y_{ij})$  are the AoA and the 2D location of TX  $j$  relative to RX  $i$  respectively. Eqn. (2) becomes a closed form expression when Lambertian models are considered, as typically done so for indoor luminaries [6]. However, since automotive head/tail light beam patterns cannot be accurately represented by a Lambertian term [22], we consider the more general Eqn. (2), which can easily be converted to an approximate Lambertian model when necessary, as done so in [11, 22].  $\tau_{ij}$  in Eqn. (1) and  $\theta_{ij}$  are expressed as:

$$\tau_{ij} = \frac{\sqrt{x_{ij}^2 + y_{ij}^2}}{c}, \quad \theta_{ij} = \arctan\left(\frac{y_{ij}}{x_{ij}}\right) \quad (3)$$

where  $c$  is the speed of light.  $\mu_i$  is composed of shot noise on the receiving p-i-n photodetector (PD) and thermal noise on the FET-based front-end transimpedance amplifier (TIA) that follows the PD [23]. The noise is zero mean, and has the following variance:

$$\sigma_{\mu_i}^2 = \sigma_{shot_i}^2 + \sigma_{thermal_i}^2 \quad (4a)$$

$$\sigma_{shot_i}^2 = 2q\gamma_i P_{r,i} B_i + 2qI_{bg,i} I_{B2} B_i \quad (4b)$$

$$\sigma_{thermal_i}^2 = 4kT_i \left( \frac{1}{R_{F,i}} I_{B2} B_i + \frac{(2\pi C_{T,i})^2}{g_{m,i}} \Gamma I_{B3} B_i^3 \right) \quad (4c)$$

where  $q$  is the Coulomb electron charge,  $P_{r,i}$  is the received optical signal power,  $I_{bg,i}$  is the background illumination current,  $B_i$  is the front-end bandwidth,  $k$  is the Boltzmann constant,  $T_i$  is the circuit temperature,  $R_{F,i}$  is the front-end resistance (i.e., TIA feedback gain term),  $C_{T,i}$  is the input capacitance due to the photodiode and the FET,  $g_{m,i}$  is the FET transconductance, and  $\Gamma$ ,  $I_{B2}$  and  $I_{B3}$  are unitless factors for FET channel noise and noise bandwidth determined by the signal shape [24]. For an optimal TIA (i.e. proper loop compensation and impedance matching such that bitrate can equal  $B_i$  [23]), Eqn. (4c) is typically reorganized using  $R_{F,i} = G/(2\pi B_i C_{T,i})$  where  $G$  is the “open-loop voltage gain”, and the front-end circuit gain is independent of transistor parameters, i.e.,  $R_{F,i}$  determines the transimpedance gain which turns the received photocurrent signal  $r_i$  into voltage.

We ignore the following minor effects: Popcorn noise due to silicon defects are absent in modern components. Flicker, i.e.,  $1/f$  noise, is also ignored since VLC operation is not near DC. Furthermore, random fluctuations on  $H_{ij}$  due atmospheric turbulence on the channel are ignored since LEDs are non-coherent. Similarly, Doppler effects, which would make  $\tau_{ij}$  time-dependent, are also ignored since they were shown to have minimal effect on positioning performance [11].

### C. VLC based Vehicle Localization

Based on this model, VLC based vehicle localization methods use the received signals, i.e.,  $r_i$ , to make observations on  $\tau_{ij}$  or  $H_{ij}$  for measuring physical system parameters, and then they use those measured parameters for estimating relative TX positions, thus, the vehicle location, via geometric relations, as depicted in Fig. 2. Positioning two TX units on the target vehicle with respect to two RX units on the ego vehicle is necessary for 2D vehicle localization [9]. However, since the two ego RX units are simply separated by  $L$ , estimating positions with respect to only RX 1, i.e.,  $(x_{11}, y_{11})$  and  $(x_{12}, y_{12})$ , is sufficient, as depicted in Fig. 1. Additionally, for longitudinally parallel vehicles only,  $(x_{12}, y_{12}) = (x_{11} + D, y_{11})$  holds and estimating only one position, i.e.,  $(x_{11}, y_{11})$  is sufficient when  $D$ , the separation between target VLC units, is known and the right/left source ambiguity can be solved.

## III. LOCALIZATION METHODS AND CRLBS

In this section we first present the details of the four state-of-the-art VLC based vehicle localization methods and derive the CRLB for each method based on their observation models.

### A. Method Descriptions

For each method, we first describe the parameter measurement procedure and then provide the geometric relations which link these parameters to TX positions; these relations constitute the observation model of the position estimators. All methods are depicted in flowchart form in Fig. 3.

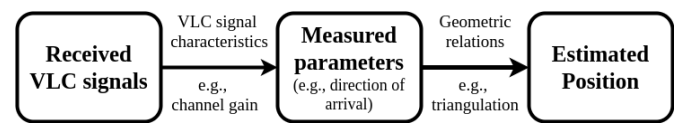


Fig. 2. The anatomy of two-step VLP algorithms.

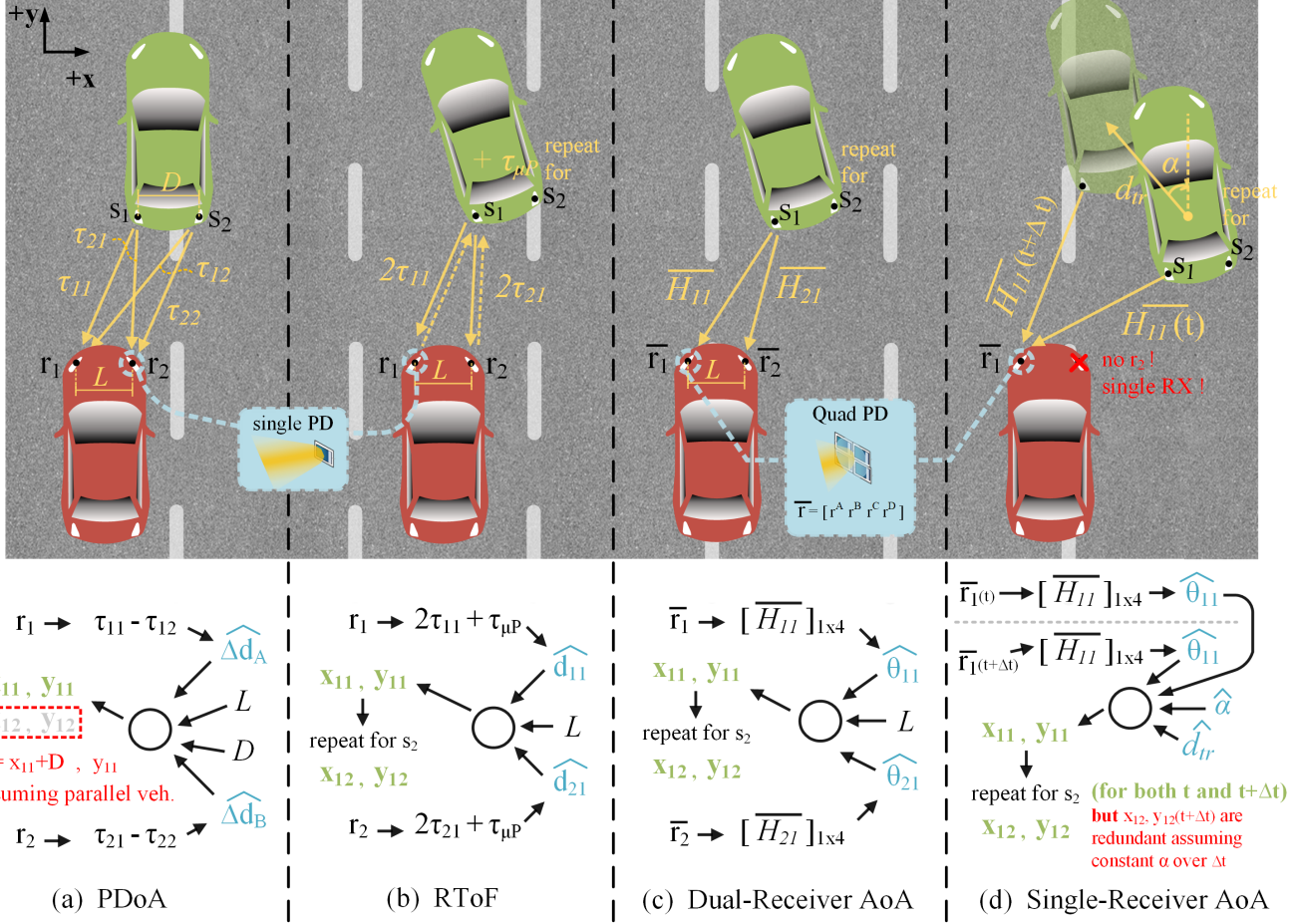


Fig. 3. Flowcharts for the methods under consideration: PDoA [10] in (a), RToF [12] in (b), dual-RX AoA [9] in (c) and single-RX AoA [13] in (d).  $L$ ,  $D$ : distances between adjacent head/tail lights for ego and target vehicles respectively.  $(\hat{d}_R, \hat{d}_L)$  and  $(\hat{\Delta d}_A, \hat{\Delta d}_B)$ : measured absolute and differences in propagation distances respectively.  $\tau_{\mu P}$ : processing time.  $\hat{\theta}_{ij}$ : measured AoA.  $\hat{\alpha}$  and  $\hat{d}_{tr}$  are measured relative heading and distance. Measured parameters used as the observations for the CRLB derivation of each method are marked in blue.

1) *Phase-Difference-of-Arrival (PDoA) Approach:* The method proposed in [10] considers the target vehicle transmitting two different constant tones of known frequency from the two TXs on one side, i.e. head or tail lights, which are received by both RXs on one side of the ego vehicle. Multiplying the upper sidebands of each of the separated  $s_1$  and  $s_2$  components in  $r_1$  with complex conjugates of their counterparts in  $r_2$  gives the difference between the propagation times of the each TX signal to both RXs [10, Eqn. 6], which is translated to measured physical parameters in the form of differences in propagation distance,  $\hat{\Delta d}_A$  and  $\hat{\Delta d}_B$  [10, Eqn. 7]:

$$\hat{\Delta d}_A = c \cdot \hat{\Delta \tau}_{11-21}, \quad \hat{\Delta d}_B = c \cdot \hat{\Delta \tau}_{12-22} \quad (5)$$

where  $\hat{\Delta \tau}_{11-21}$  and  $\hat{\Delta \tau}_{12-22}$  are the measured differences between the propagation times from each TX to the two RXs. Assuming longitudinally parallel vehicles, these measured parameters can be used for estimating left target TX unit position, i.e.,  $(x_{1,1}, y_{1,1})$ , based on the following set of geometric relations, which constitutes the observation model:

$$\Delta d_A = \sqrt{x_{11}^2 + y_{11}^2} - \sqrt{(x_{11} + D)^2 + y_{11}^2} \quad (6a)$$

$$\Delta d_B = \sqrt{(x_{11} - L)^2 + y_{11}^2} - \sqrt{(x_{11} - L + D)^2 + y_{11}^2} \quad (6b)$$

where  $D$ , separation between the two lights on the target vehicle, is also assumed to be known. Since  $(x_{12}, y_{12}) = (x_{11} + D, y_{11})$  as explained in Section II-C due to the parallel, the observation model becomes rank-deficient for independent estimation of all 4 coordinates. Therefore, Eqn. (6) and the estimator output for CRLB analysis only consists of  $(x_{11}, y_{11})$  given observations  $\hat{\Delta d}_A$  and  $\hat{\Delta d}_B$  from two RXs, and the constants  $L$  and  $D$ , for longitudinally parallel vehicles.

2) *Roundtrip-Time-of-Flight (RToF) Approach:* The method proposed in [11] considers the ego vehicle transmitting a waveform of center frequency  $f_e$ , which gets detected, amplified and retransmitted back to the ego vehicle by the target vehicle. The initial TX signal and the final RX signal are downconverted and filtered via heterodyning and the time difference between them are digitally measured after zero-crossing detection. After subtracting the known processing time offset  $\tau_{\mu P}$  from the measured time difference, the result is converted to the distance between the respective TX and the RX via dividing by the speed of light. This procedure is repeated for both TX units and both RX units to position both TXs on the target vehicle. We reduce the phase measurement equation in [11, Eqn. 7] to an observation on  $\tau_{ij}$  for clarity and express these measured parameters as:

$$\widehat{d}_{ij} = c(\widehat{\tau}_{ij}) , \quad \widehat{\tau}_{ij} = \frac{\widehat{\varphi}}{(2f_e)(2\pi)} - \tau_{\mu P} \quad (7)$$

where  $\widehat{d}_{ij}$  are measured propagation distance parameters, where  $i, j \in \{1, 2\}$ , and  $\widehat{\varphi}$  is the measured phase difference. The positions of both TX units are estimated using these measured parameters based on the following geometric relations, which constitute the observation model:

$$d_{ij} = \begin{cases} \sqrt{x_{1j}^2 + y_{1j}^2} , & \text{if } i = 1 \\ \sqrt{(x_{1j} - L)^2 + y_{1j}^2} , & \text{if } i = 2 \end{cases} \quad (8)$$

where  $j \in \{1, 2\}$ . Hence, the estimator outputs  $(x_{11}, y_{11})$  and  $(x_{12}, y_{12})$  (i.e., no parallel vehicles assumption) given the four observations  $\widehat{d}_{ij}$  from two RXs, and the constant  $L$ .

3) *Dual Receiver Angle-of-Arrival (AoA2) Approach:* The method proposed in [9] considers an RX that uses a quadrant photodiode (QRX), rather than a single photodiode as in PDoA and RToF. The ratio of channel gains  $H_{ij}$  from a given TX  $j$  to each of the four cells in QRX  $i$  is determined jointly by the AoA of TX  $j$  to QRX  $i$  and the optical configuration of the QRX. Therefore, since the optical configuration is known and the received signals at each of the closely-packed cells have very similar propagation delays, the AoA from each TX to each QRX can be estimated as [9, Eqn. 6]

$$\widehat{\theta}_{ij} = g_{QRX} \left( \widehat{H}_{ij} \right) \quad (9)$$

where  $\widehat{H}_{ij}$  is the  $1 \times 4$  vector containing the observations on  $H_{ij}$  for all cells of QRX  $i$ ,  $i, j \in \{1, 2\}$ , and  $g_{QRX}$  is the optical function translating  $\widehat{H}_{ij}$  into the measured AoA parameters. Note that true values of  $H_{ij}$  are not estimated, rather, relative proportions of  $H_{ij}$  values are used for AoA measurement; this alleviates the need for complex channel estimation techniques. The method uses these measured AoA parameters for positioning the two TXs based on the following geometric relations, which constitute the observation model:

$$\theta_{ij} = \begin{cases} \arctan \left( \frac{y_{1j}}{x_{1j}} \right) , & \text{if } i = 1 \\ \arctan \left( \frac{y_{1j}}{x_{1j} - L} \right) , & \text{if } i = 2 \end{cases} \quad (10)$$

where  $j \in \{1, 2\}$ . Hence, the estimator outputs  $(x_{11}, y_{11})$  and  $(x_{12}, y_{12})$  given the four observations  $\widehat{\theta}_{ij}$  from two QRXs, and the constant  $L$ .

4) *Single Receiver Angle-of-Arrival (AoA1) Approach:* The method proposed in [13] uses the same QRX as in [9] for AoA measurement from received signals but uses only a single QRX. Two time-consecutive AoA measurements separated by a  $\Delta t$  for both target TXs to a single QRX, i.e.,  $\theta_{1j}(t)$  and  $\theta_{1j}(t + \Delta t)$  where  $j \in \{1, 2\}$ , the relative heading of the target vehicle during that interval,  $\alpha$ , and the relative distance travelled by the target vehicle during that interval,  $d_{tr}$ , are used for positioning both TX units. While the AoA measurement in Eqn. (9) is used directly with  $i = 1$ ,  $\alpha$  and  $d_{tr}$  are measured using vehicle sensor data as follows [13, Eqns. (1) and (2)]:

$$\widehat{\alpha} = \frac{\pi}{2} - \arctan \left( \frac{d_{tt} \cdot \cos(\psi) - d_{rr}}{d_{tt} \cdot \sin(\psi)} \right) \quad (11a)$$

$$\widehat{d}_{tr} = \sqrt{(d_{tt} \cdot \cos(\psi))^2 + (d_{tt} \cdot \sin(\psi) - d_{rr})^2} \quad (11b)$$

where  $d_{tt}$  and  $d_{rr}$  are the absolute distances traveled by the target and ego vehicles respectively, and  $\psi$  is the difference between the global headings of target and ego vehicles with respect to true north.  $d_{tt}$ ,  $d_{rr}$  and  $\psi$  are measured by vehicle sensors and target vehicle quantities are transmitted to the ego vehicle over the VLC link. Assuming that  $\alpha$  is constant over the  $\Delta t$  period, the geometric relations that govern the observation model for this estimator are:

$$\theta_{1j}(t) = \arctan \left( \frac{y_{1j}(t)}{x_{1j}(t)} \right) \quad (12a)$$

$$\theta_{1j}(t + \Delta t) = \arctan \left( \frac{y_{1j}(t + \Delta t)}{x_{1j}(t + \Delta t)} \right) \quad (12b)$$

$$\alpha = \arctan \left( \frac{d_x}{d_y} \right) , \quad d_{tr} = \sqrt{(d_x)^2 + (d_y)^2} \quad (12c)$$

where  $j \in \{1, 2\}$  and  $d_x$  and  $d_y$  are distances traveled by the target vehicle relative to the ego vehicle in x and y directions during the  $\Delta t$  interval respectively, which are expressed as:

$$d_x = x_{11}(t + \Delta t) - x_{11}(t) \quad (13a)$$

$$d_y = y_{11}(t + \Delta t) - y_{11}(t) . \quad (13b)$$

Note that while this method provides two TX position estimations for two times instants, since constant  $\alpha$  over  $\Delta t$  is assumed, one (x,y) tuple, e.g.,  $(x_{12}(t + \Delta t), y_{12}(t + \Delta t))$ , can be expressed as a combination of the other six estimated coordinates, making the eight coordinate estimation problem rank deficient. Therefore, Eqn. (12) and the estimator output for CRLB analysis consists of the six coordinates  $(x_{1j}(t), y_{1j}(t))$  and  $(x_{11}(t + \Delta t), y_{11}(t + \Delta t))$  given the six observations  $\theta_{1j}(t)$  and  $\theta_{1j}(t + \Delta t)$ ,  $\widehat{\alpha}$  and  $\widehat{d}_{tr}$ , where  $j \in \{1, 2\}$ , from a single ego QRX and heading and speed sensors on both vehicles.

## B. Cramer-Rao Lower Bounds

In this section, we first summarize the Cramer-Rao lower bound derivation procedure for an arbitrary system in AWGN noise and then apply that procedure to the observation models for each of the four VLC based localization methods.

An unbiased estimator of  $\mathbf{P}_{1 \times N_M}$  is considered, which uses observations  $\mathbf{M}_{1 \times N_H}$  for a system  $\mathbf{G}_{1 \times N_H}$  in zero-mean AWGN  $\mathbf{W}_{1 \times N_H}$  with variance  $\sigma_{\mathbf{W}}^2$ , described by

$$M_h = G_h(\mathbf{P}) + W_h , \quad h = 0, 1, \dots, N_H \quad (14)$$

where  $m$  and  $h$  denotes indexes,  $N_H$  is the number of observations and  $N_M$  is the number of parameters to be estimated. As per Eqn. (14), the CRLB on the mean squared error of an unbiased estimator for each element of  $\mathbf{P}$ , i.e.,  $\widehat{P}_m$  where  $m \in \{1, 2, \dots, N_M\}$ , is lower-bounded by

$$\text{var}(\widehat{P}_m) \geq (\mathbf{F}^{-1})_{m,m} \quad (15)$$

where  $\mathbf{F}$  is the Fisher information matrix (FIM) defined as

$$\mathbf{F} = E[ (\nabla_{\mathbf{P}} \ln(p(\mathbf{M}|\mathbf{P}))) (\nabla_{\mathbf{P}} \ln(p(\mathbf{M}|\mathbf{P})))^T ], \quad (16)$$

where  $p$  is likelihood and  $E$  is expectation. Since each observation  $M_h$  is an independent Gaussian random variable with mean  $G_h(\mathbf{P})$  and variance  $\sigma_{W_h}^2$ , the expression for elements  $(m, m')$  of the FIM simplifies to [25, Ch. 3.9]:

$$\mathbf{F}_{m,m'} = - \sum_{h=1}^{N_h} \frac{1}{\sigma_{W_h}^2} \left( \frac{\delta G_h(\mathbf{P})}{\delta P_m} \cdot \frac{\delta G_h(\mathbf{P})}{\delta P_{m'}} \right) \quad (17)$$

where  $m \in \{1, 2, \dots, N_M\}$ . This procedure is applicable to the observation models of all described methods for obtaining their respective CRLBs on unbiased position estimation accuracy with respect to measured noisy parameters by Eqn. (15). However, since the exact symbolic expressions for the CRLBs do not provide any extra intuition and are significantly long and complex due to the matrix inversion in Eqn. (15), we rather present here the derivative terms in Eqn. (17) for each method. The FIM can then be evaluated and the numerical value of the CRLB for a given condition, i.e., given  $\mathbf{P}$  and  $\mathbf{W}$ , can be obtained easily as per Eqn. (15).

As clarification for the noise term  $\mathbf{W}$ : Since all parameter measurement expressions, i.e., Eqns. (5), (7), (9) and (11), are smooth, thus, piece-wise linear functions for feasibly small standard deviations of  $\mu_i$ , we assume all measured parameters also experience AWGN, i.e., we assume  $\mathbf{W}$  is zero mean AWGN with variance  $\sigma_{\mathbf{W}}^2$  which is the output variance of the respective parameter measurement procedures (Eqns. (5), (7), (9) and (11)) for a given  $\mu_i$  at their inputs. This phenomenon, i.e., an approximately Gaussian output for an AWGN input of a system that is piece-wise linear for relatively small input standard deviations, is thoroughly described in [25, Ch. 3.6], and it enables using Eqn. (17) for all discussed methods.

1) *Phase-Difference-of-Arrival (PDoA) Approach:* For the PDoA approach, the terms in Eqn. (14) are defined as

$$\mathbf{G} = [\Delta_{dA} \ \Delta_{dB}] = \mathbf{G}(\mathbf{P}, L, D) \quad (18a)$$

$$\mathbf{P} = [x_{11} \ y_{11}] \quad (18b)$$

where  $\mathbf{G}(\mathbf{P}, L, D)$  is described by Eqn. (6) and  $\mathbf{M}$  simply consists of noisy observations of  $\mathbf{G}$ , i.e.,  $\widehat{\mathbf{G}} = [\widehat{\Delta}_{dA} \ \widehat{\Delta}_{dB}]$ . For constructing the 2x2 FIM for the PDoA method with respect to Eqn. (17), we provide the following derivative terms:

$$\frac{\delta \Delta_{dA}}{\delta x_{11}} = f_1(x_{11}) - f_1(x_{11} + D) \quad (19a)$$

$$\frac{\delta \Delta_{dB}}{\delta x_{11}} = f_1(x_{11} - L) - f_1(x_{11} - L + D) \quad (19b)$$

$$\frac{\delta \Delta_{dA}}{\delta y_{11}} = y_{11} ( f_2(x_{11}) - f_2(x_{11} + D) ) \quad (19c)$$

$$\frac{\delta \Delta_{dB}}{\delta y_{11}} = y_{11} ( f_2(x_{11} - L) - f_2(x_{11} - L + D) ) \quad (19d)$$

$$f_1(x) = x \cdot f_2(x) = \frac{x}{\sqrt{x^2 + y_{11}^2}} . \quad (19e)$$

Note that the 4x4 FIM for this method, i.e., the FIM for when  $(x_{12}, y_{12})$  are included in  $\mathbf{P}$ , results in a rank-deficient, thus, non-invertible matrix as discussed in Section III-A-1. Therefore, the CRLB for this method only exists when the two vehicles are longitudinally parallel, i.e., when the FIM is 2x2. This theoretically proves the necessity of the parallel vehicles assumption for the forward pass of this method.

2) *Roundtrip-Time-of-Flight (RToF) Approach:* We repeat the same procedure for the RToF approach. The terms in Eqn. (14) are defined as

$$\mathbf{G} = [d_{11} \ d_{12} \ d_{21} \ d_{22}] = \mathbf{G}(\mathbf{P}, L) \quad (20a)$$

$$\mathbf{P} = [x_{11} \ y_{11} \ x_{12} \ y_{12}] \quad (20b)$$

where  $\mathbf{M}$  consists of noisy observations of  $\mathbf{G}$ , and  $\mathbf{G}(\mathbf{P}, L)$  is described by Eqn. (8). The derivative expressions used for constructing the 4x4 FIM as per Eqn. (17) are:

$$\frac{\delta d_{1j}}{\delta x_{1j}} = \frac{x_{1j}}{\sqrt{x_{1j}^2 + y_{1j}^2}}, \quad \frac{\delta d_{1j}}{\delta y_{1j}} = \frac{y_{1j}}{\sqrt{x_{1j}^2 + y_{1j}^2}} \quad (21a)$$

$$\frac{\delta d_{2j}}{\delta x_{1j}} = \frac{x_{1j} - L}{\sqrt{(x_{1j} - L)^2 + y_{1j}^2}}, \quad \frac{\delta d_{2j}}{\delta y_{1j}} = \frac{y_{1j}}{\sqrt{(x_{1j} - L)^2 + y_{1j}^2}} \quad (21b)$$

where  $j \in \{1, 2\}$  and all other derivative terms are zero.

3) *Dual Receiver Angle-of-Arrival (AoA2) Approach:* We repeat the same procedure for the dual-RX AoA approach. The terms in Eqn. (14) are defined as

$$\mathbf{G} = [\theta_{11} \ \theta_{12} \ \theta_{21} \ \theta_{22}] = \mathbf{G}(\mathbf{P}, L) \quad (22a)$$

where  $\mathbf{P}$  is the same as in Eqn. (20b),  $\mathbf{G}(\mathbf{P}, L)$  is described by Eqn. (10) and  $\mathbf{M}$  consists of noisy observations of  $\mathbf{G}$ . The derivative expressions used for constructing the 4x4 FIM are:

$$\frac{\delta \theta_{1j}}{\delta x_{1j}} = \frac{-y_{1j}}{\sqrt{x_{1j}^2 + y_{1j}^2}}, \quad \frac{\delta \theta_{1j}}{\delta y_{1j}} = \frac{x_{1j}}{\sqrt{x_{1j}^2 + y_{1j}^2}} \quad (23a)$$

$$\frac{\delta \theta_{2j}}{\delta x_{1j}} = \frac{-y_{1j}}{(x_{1j} - L)^2 + y_{1j}^2}, \quad \frac{\delta \theta_{2j}}{\delta y_{1j}} = \frac{(x_{1j} - L)}{(x_{1j} - L)^2 + y_{1j}^2} \quad (23b)$$

where  $j \in \{1, 2\}$  and all other derivative terms are zero.

4) *Single Receiver Angle-of-Arrival (AoA1) Approach:* We repeat the same procedure for the single-RX AoA approach. The terms in Eqn. (14) are defined as

$$\mathbf{G} = [\theta_{11}(t) \ \theta_{11}(t+\Delta t) \ \theta_{12}(t) \ \theta_{12}(t+\Delta t) \ \alpha \ d_{tr}] \quad (24a)$$

$$\mathbf{P} = [A_{11}(t) \ A_{11}(t)(t+\Delta t) \ A_{12}(t)] \quad (24b)$$

$$\mathbf{A}_{ij}(t) = [ \ x_{ij}(t) \ y_{ij}(t) \ ] \quad (24c)$$

where  $\mathbf{M}$  consists of noisy observations of  $\mathbf{G}$ , and  $\mathbf{G}(\mathbf{P}, L)$  is described by Eqns. (12) and (13). The terms for  $\theta_{1,j}(t)$  and  $\theta_{1,j}(t+\Delta t)$ ,  $j \in \{1, 2\}$ , are the same as in Eqn. (23a) and the derivation of the terms for  $\alpha$  and  $d_{tr}$  are straightforward using the previously derived primitives. Note that the terms  $x_{12}(t+\Delta t)$  and  $y_{12}(t+\Delta t)$  are excluded since they make the FIM rank deficient because they can be computed as combinations of the other six terms in  $\mathbf{P}$  as explained in Section III-A-4. This theoretically proves the necessity of the constant vehicle heading assumption for this method.

#### IV. NUMERICAL RESULTS

In this section we evaluate the derived CRLBs for each method under three realistic driving scenarios: platooning on a straight highway, joining a platoon from an adjacent lane, and collision avoidance during a dangerous lane change maneuver. We first simulate the parameter measurement procedures of each method for each scenario and channel condition, run this multiple times, and sample the output variance in parameter measurement,  $\sigma_w^2$ . Afterwards we use  $\sigma_w^2$  values in Eqn. (17) for computing the FIM, thus, the CRLB for each method, using Eqn. (15). For all three scenarios, we present the square root of the CRLBs, i.e., standard deviation of the zero-mean unbiased position estimation error, for only  $(x_{11}, y_{11})$  since results for  $(x_{12}, y_{12})$  are similar. We do not investigate PDoA and AoA1 methods for the scenarios that do not consider longitudinally parallel vehicles and constant relative vehicle headings, respectively, since these methods have systematic error, i.e., non-zero bias when these assumptions are violated, and CRLB only applies to unbiased estimators.

For fair comparison, we use the same simulation setup for all methods: estimation rate is 200 Hz and QRXs in [9] are used, but RToF and PDoA methods use the sum of the photocurrents from the four cells of QRX  $i$  as  $r_i$ , and AoA1 and AoA2 methods use each cell separately; this ensures equivalent signal-to-noise-ratios (SNR) among all methods. The TIA noise-equivalent bandwidth and the clock/sampling rate is assumed to be 10 MHz (i.e., RToF  $f_{clock}=10$  MHz in [11, Eqn. (3)]). TXs 1 and 2 transmit constant tones of 1 MHz and 900 KHz respectively; the only signals supported by all methods without compromise are constant tones, and  $\leq 1$  MHz is feasible for current commercially available automotive LEDs [11]. TXs are typical taillights with 1 W optical power each and beam patterns approximated by a Lambertian term of 20° half-power angle (order  $m=11$ ) as in [11]. Two channel conditions are considered: low noise and high noise, which respectively correspond to low ambient light, cold temperature nighttime conditions and daytime conditions with moderate temperature and ambient sunlight as quantified in [26]. All simulator setup parameters are summarized in Table I.

TABLE I  
SIMULATOR SETUP PARAMETERS

VLC TX	Signal	constant tones: 0.90 MHz and 1.00 MHz
	Power	$\gamma_j \cdot \max( s_j ) = 1$ W (typical tail light)
	Pattern [11]	Lambertian, $m = \frac{-\ln 2}{\ln(\cos(20^\circ))} = 11$
VLC QRX	$\gamma_i, g_m$	0.5 A/W, 30 mS
	$A_i$ (active)	50 mm <sup>2</sup> , total area for 4 cells
	$B, C_T, R_F$	10 MHz, 56 pF, 2.84 kΩ, i.e., $G \approx 10$
	Factors	$\Gamma=1.5, I_{B2}=0.562, I_{B3}=0.0868$
	FoV	$\pm 80^\circ$ , as in [9]
	$I_{bg}$ [26], $T$	low noise: $I_{bg}=10 \mu\text{A}, T=273 \text{ K}$ high noise: $I_{bg}=750 \mu\text{A}, T=298 \text{ K}$
Vehicle	Dimensions	Length = 5 m. $L, D = 1.6$ m
	Steering	Ackermann [27] (small sideslip angles)

#### A. Scenario 1 - Straight Highway Platooning, Long Range

Fig. 4 demonstrates the performances of all methods for a typical highway platooning scenario where a target vehicle is leading an ego vehicle vehicle on the same lane and both vehicles are driving straight, longitudinally parallel to each other. In order to demonstrate performance at different distances, the target vehicle moves away from the ego vehicle starting at 5 m, ending at 18 m longitudinal distance. All methods perform unbiased estimation under these conditions, but only RToF and AoA2 can provide 2D position estimation at cm-level accuracy under low noise conditions and at  $>10$  cm accuracy under high noise conditions up to  $\approx 12$  m distance. None of the methods can provide cm-level 2D positioning accuracy for longer distances under high noise conditions: AoA1 generally shows resilience against high noise since the heading and speed sensor data it incorporates does not get contaminated by VLC channel noise and provides cm-level lateral positioning, but it fails to sustain the same for the longitudinal axis, thus, fails to provide cm-level 2D accuracy for long distances. RToF shows cm-level longitudinal accuracy, but cannot sustain this for the lateral axis, thus, fails to provide cm-level 2D accuracy for long distances under high noise.

These results demonstrate that RToF and AoA2 provide sufficient accuracy for long-distance platooning on straight highways under low to moderate noise, and that the PDoA method cannot provide cm-level accuracy under any realistic condition: While it is known that the accuracy of this PDoA method improves with higher frequency [10], this is not feasible with current automotive LEDs, and since the PDoA method cannot provide estimation without systematic error in the other scenarios that consider non-parallel vehicles, we conclude that it is not feasible for use in platooning and collision avoidance with current automotive LED technology.

#### B. Scenario 2 - Joining a Highway Platoon, Close Range

Fig. 5 demonstrates results for RToF, AoA2 and AoA1 in a platoon formation scenario where a target vehicle joins the platoon as a new leader by moving in front of the ego vehicle, which becomes the follower. The PDoA method is not considered here since the vehicles are not parallel. All three methods demonstrate  $\leq 30$  cm 2D position estimation accuracy under low noise conditions. AoA1 additionally shows resilience against high noise and sustains this performance under high noise conditions while RToF and AoA2 remain in the [30, 100] cm band for the same conditions. These results demonstrate that the RToF, AoA2 and AoA1 methods provide sufficient accuracy for close-range miscellaneous platoon scenarios under low to moderate noise conditions and that AoA1 can sustain this for also high noise conditions.

#### C. Scenario 3 - Highway Collision Avoidance

Fig. 6 demonstrates results for RToF and AoA2 methods in a typical collision avoidance scenario where a target vehicle on the leftmost lane leading the ego vehicle on the center lane brakes heavily during a lane change maneuver towards the rightmost lane and risks a collision. The PDoA method is not considered here since the vehicles are not parallel, and the AoA1 method is not considered since the target

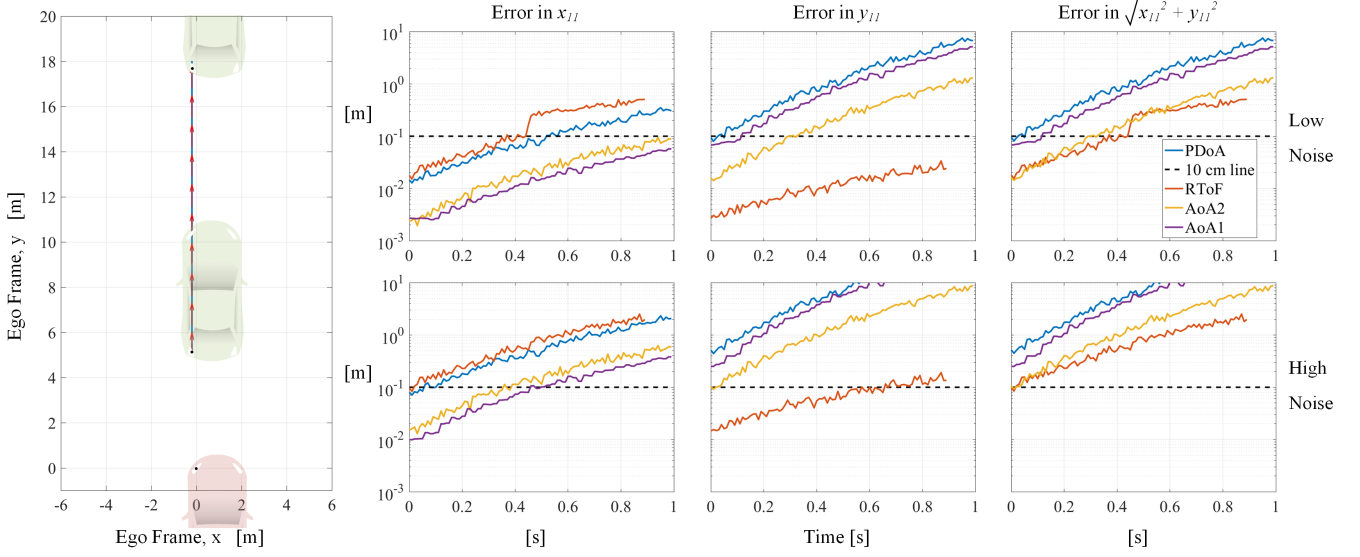


Fig. 4. *Scenario 1* - Platooning on a straight highway, longitudinally parallel vehicles. Target starts from 5 m away from ego and ends at 18 m away. Red quiver arrows denote instantaneous target vehicle heading and blue track denotes relative target vehicle trajectory in ego vehicle frame.

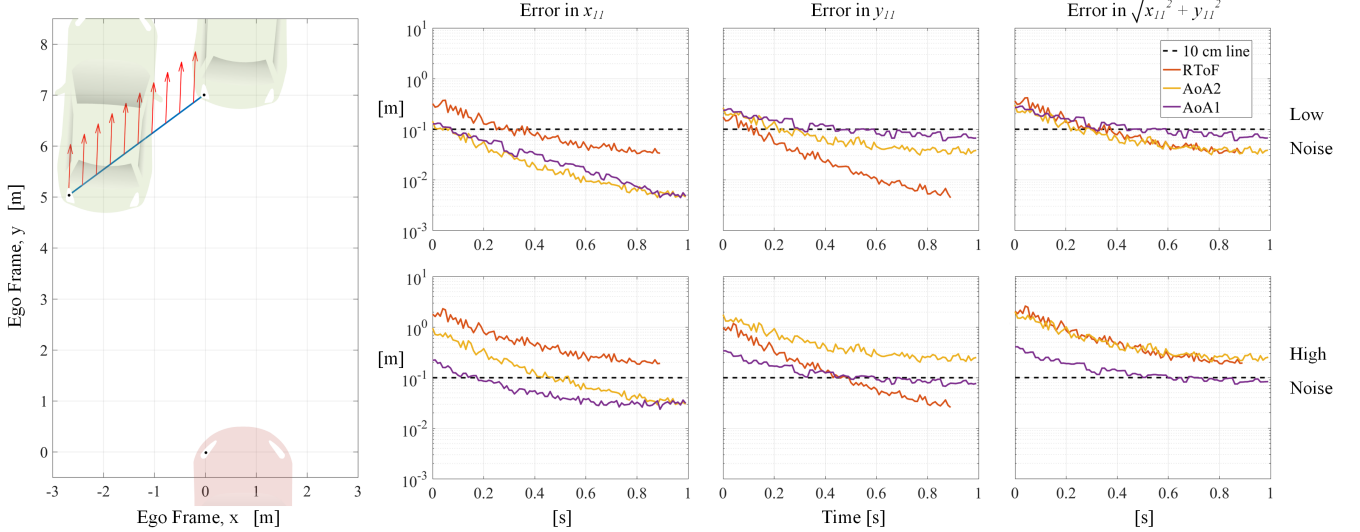


Fig. 5. *Scenario 2* - Joining a highway platoon. Target vehicle moves in front of the ego vehicle. Vehicles are not parallel, but have constant heading difference. Red quiver arrows denote instantaneous target vehicle heading and blue track denotes relative target vehicle trajectory in ego vehicle frame.

vehicle heading changes dynamically. Both RTToF and AoA2 methods show cm-level accuracy for majority of the trajectory under both low and high noise conditions with AoA2 performance generally surpassing RTToF performance. However, performance is tightly dependent on relative vehicle heading for this scenario: Due to the narrow beam pattern of the TX taillight, the target TX beam “points away from” the ego RX active area for certain relative headings, which severely decreases SNR, thus, decreases performance. This effect is visible in all conditions where accuracy degrades up until the 0.2 s mark even though the target vehicle is getting closer.

These results demonstrate that RTToF and AoA2 methods can provide sufficient accuracy for collision avoidance but performance heavily depends on the relative headings of the vehicles since the narrow-beam TX vehicle lights may instantaneously “point away from” the ego RXs, severely decreasing accuracy.

## V. CONCLUSION

This paper provides the theoretical performance analysis and fair comparison of four state-of-the-art VLC-based vehicle localization methods which respectively utilize the PDoA, RTToF and single/dual RX AoA (AoA1/AoA2) characteristics of VLC signals for two-step positioning of TXs on head/tail LED lights (i.e., physical parameter measurement + geometric position estimation). Specifically, we derive the CRLB on positioning accuracy for the geometric relations utilized by each method with respect to their input physical parameters (i.e., observation models), simulate their proposed parameter measurement procedures under platooning and collision avoidance scenarios that consider realistic noise conditions, and evaluate the derived CRLBs using these simulated measurements for fair comparison. Since the CRLBs are derived using measured parameters as observations, they apply to all VLC-based

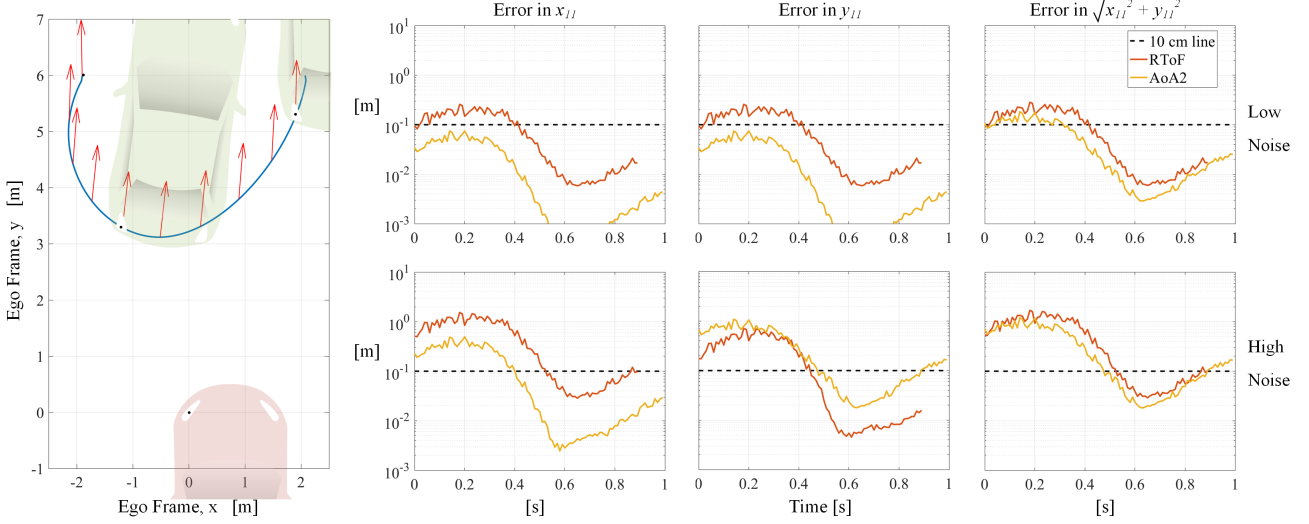


Fig. 6. Scenario 3 - A typical dangerous lane change maneuver motivating collision avoidance systems, where the target vehicle brakes heavily while crossing towards the lane to the right of the ego vehicle. Vehicles are not longitudinally parallel and their relative heading varies throughout the scenario. Red quiver arrows denote instantaneous target vehicle heading and blue track denotes relative target vehicle trajectory in ego vehicle frame.

vehicle localization methods that use the same geometries (i.e., with different parameter measurement procedures).

Results show that the PDoA based method cannot provide the required cm-level accuracy under realistic conditions since it requires  $\geq 10$  MHz LED bandwidth. The AoA1 method provides cm-level accuracy for close range platooning, but is inaccurate at high distances due to a high-sensitivity geometry. RToF and AoA2 methods provide cm-level accuracy under moderate VLC channel noise for all scenarios within 10 m distance, theoretically proving the feasibility of VLC based vehicle localization for collision avoidance and platooning.

## REFERENCES

- [1] Ford Motor Company, “A matter of trust: Ford’s approach to developing self-driving vehicles,” 16 Aug 2018, press Release.
- [2] D. Caveney, “Cooperative vehicular safety applications,” *IEEE Control Syst. Mag.*, vol. 30, no. 4, pp. 38–53, 2010.
- [3] S. E. Shladover and S.-K. Tan, “Analysis of vehicle positioning accuracy requirements for communication-based cooperative collision warning,” *Journal of Intelligent Transportation Systems*, vol. 10, no. 3, pp. 131–140, 2006.
- [4] F. de Ponte Müller, “Survey on ranging sensors and cooperative techniques for relative positioning of vehicles,” *Sensors*, vol. 17, no. 2, p. 271, 2017.
- [5] J. Armstrong, Y. A. Sekercioglu, and A. Neild, “Visible light positioning: a roadmap for international standardization,” *IEEE Communications Magazine*, vol. 51, no. 12, pp. 68–73, 2013.
- [6] H. Steendam, T. Q. Wang, and J. Armstrong, “Cramer-Rao bound for indoor visible light positioning using an aperture-based angular-diversity receiver,” in *2016 IEEE International Conference on Communications (ICC)*. IEEE, 2016, pp. 1–6.
- [7] S. Lee, J. K. Kwon, S.-Y. Jung, and Y.-H. Kwon, “Evaluation of visible light communication channel delay profiles for automotive applications,” *EURASIP journal on Wireless Communications and Networking*, vol. 2012, no. 1, p. 370, 2012.
- [8] B. Turan, G. Gurbilek, A. Uyurus, and S. C. Ergen, “Vehicular vlc frequency domain channel sounding and characterization,” in *2018 IEEE Vehicular Networking Conference (VNC)*. IEEE, 2018, pp. 1–8.
- [9] B. Soner and S. Coleri, “Visible Light Communication based Vehicle Localization and Pose Estimation,” 29 Sep 2020, arXiv pre-print.
- [10] R. Roberts, P. Gopalakrishnan, and S. Rathi, “Visible light positioning: Automotive use case,” in *2010 IEEE Vehicular Networking Conference*. IEEE, 2010, pp. 309–314.
- [11] B. Béchadergue, L. Chassagne, and H. Guan, “Visible light phase-shift rangefinder for platooning applications,” in *2016 IEEE 19th International Conference on Intelligent Transportation Systems (ITSC)*. IEEE, 2016, pp. 2462–2468.
- [12] ———, “A visible light-based system for automotive relative positioning,” in *2017 IEEE SENSORS*. IEEE, 2017, pp. 1–3.
- [13] B. Soner and S. C. Ergen, “Vehicular visible light positioning with a single receiver,” in *2019 IEEE 30th Annual International Symposium on Personal, Indoor and Mobile Radio Communications (PIMRC)*. IEEE, 2019, pp. 1–6.
- [14] M. F. Keskin and S. Gezici, “Comparative theoretical analysis of distance estimation in visible light positioning systems,” *Journal of Lightwave Technology*, vol. 34, no. 3, pp. 854–865, 2016.
- [15] H. Wu, S. Cheng, Y. Peng, K. Long, and J. Ma, “IEEE 802.11 distributed coordination function (DCF): analysis and enhancement,” in *2002 IEEE International Conference on Communications. Conference Proceedings. ICC 2002 (Cat. No. 02CH37333)*, vol. 1. IEEE, 2002, pp. 605–609.
- [16] K. D. Kusano and H. C. Gabler, “Safety benefits of forward collision warning, brake assist, and autonomous braking systems in rear-end collisions,” *IEEE Trans. Intell. Transp. Syst.*, vol. 13, no. 4, pp. 1546–1555, 2012.
- [17] American Association of Highway and Transportation Officials (AASHTO), “Chapter 3.4.6: Vertical curves,” in *A Policy on Geometric Design of Highways and Streets, 7th edition*, 2011, pp. 295–310.
- [18] “Recommendation on the Photometry of Marine Aids to Navigation Signal Lights, Section 2.4,” AISM/IALA E-122, Saint Germain en Laye, FR, Recommendation, Jun. 2001.
- [19] S.-H. Ma, C.-H. Lee, and C.-H. Yang, “Achromatic led-based projection lens design for automobile headlamp,” *Optik*, vol. 191, pp. 89–99, 2019.
- [20] V. Jacobs, S. Forment, P. Rombauts, and P. Hanselaer, “Near-field and far-field goniophotometry of narrow-beam led arrays,” *Lighting Research & Technology*, vol. 47, no. 4, pp. 470–482, 2015.
- [21] R. J. Mathar, “Solid angle of a rectangular plate,” *Max-Planck Institute of Astronomy*, pp. 1–9, 2015.
- [22] W. Viriyasitavat, S.-H. Yu, and H.-M. Tsai, “Short paper: Channel model for visible light communications using off-the-shelf scooter taillight,” in *2013 IEEE Vehicular Networking Conference*. IEEE, 2013, pp. 170–173.
- [23] R. Smith and S. Personick, “Receiver design for optical fiber communication systems,” in *Semiconductor devices for optical communication*. Springer, 1980, pp. 89–160.
- [24] J. M. Kahn and J. R. Barry, “Wireless infrared communications,” *Proceedings of the IEEE*, vol. 85, no. 2, pp. 265–298, 1997.
- [25] S. M. Kay, *Fundamentals of statistical signal processing*. Prentice Hall PTR, 1993.
- [26] A. J. Moreira, R. T. Valadas, and A. de Oliveira Duarte, “Optical interference produced by artificial light,” *Wireless Networks*, vol. 3, no. 2, pp. 131–140, 1997.
- [27] J. Ackermann, “Robust decoupling of car steering dynamics with arbitrary mass distribution,” in *Proceedings of 1994 American Control Conference-ACC’94*, vol. 2. IEEE, 1994, pp. 1964–1968.